Detection of Electrically Modulated Inverse Spin Hall Effect in an Fe/GaAs Microdevice

K. Olejník, J. Wunderlich, A. C. Irvine, R. P. Campion, V. P. Amin, Jairo Sinova, and T. Jungwirth

Phys. Rev. Lett. **109**, 076601 — Published 15 August 2012

DOI: 10.1103/PhysRevLett.109.076601

Detection of electrically modulated inverse spin Hall effect in Fe/GaAs microdevice

K. Olejník,[1, 2] J. Wunderlich,[2, 1] A. C. Irvine,[3] R. P. Campion,[4] V. P. Amin,[5] Jairo Sinova,[5, 2] and T. Jungwirth[2, 4]

[1]*Hitachi Cambridge Laboratory, Cambridge CB3 0HE, United Kingdom*
[2]*Institute of Physics ASCR, v.v.i., Cukrovarnická 10, 162 53 Praha 6, Czech Republic*
[3]*Microelectronics Research Centre, Cavendish Laboratory, University of Cambridge, CB3 0HE, United Kingdom*
[4]*School of Physics and Astronomy, University of Nottingham, Nottingham NG7 2RD, United Kingdom*
[5]*Department of Physics, Texas A&M University, College Station, TX 77843-4242, USA*

We report detection of the inverse spin Hall effect in n-GaAs combined with electrical injection and modulation of the spin-current. We use epitaxial ultrathin-Fe/GaAs injection contacts with strong in-plane magnetic anisotropy. This allows us to simultaneously perform Hanle spin-precession measurements on Fe detection electrode and inverse spin Hall effect measurements in applied in-plane hard-axis magnetic field. In this geometry we can experimentally separate the ordinary from the spin-Hall signals. Electrical spin injection and detection is combined in our microdevice with an applied electrical drift current to modulate the spin distribution and spin current in the channel. The magnitudes and external field dependencies of the signals are quantitatively modeled by solving drift-diffusion and Hall-cross response equations.

PACS numbers: 72.25.Dc, 72.25.Hg, 85.75.Nn

The realization of information processing devices based on the electron spin fuels intense research of three key elements: injection, detection, and manipulation of spins in semiconductors. Electrical detection by the inverse spin Hall effect (iSHE) and manipulation by a gate-voltage dependent spin-orbit field was combined with optical spin injection in a 2D GaAs [1, 2] and led to an experimental demonstration of a spin dependent logic device [2]. Spin detection by iSHE is a favorable method as it allows to measure spin-current electrically and non-destructively without using magnetic elements [1]. In the direct spin Hall effect (SHE), an unpolarized electrical current leads to a transverse spin-current with out-of-plane polarization due to the spin-orbit coupling [3–11]. In iSHE [1, 4, 12–15], the spin-current generates a transverse current of charge and can be detected electrically.

Several recent works have used Fe/GaAs semiconductor Schottky contacts for electrical spin injection and detection by the non-local spin valve effect [16–21]. We have designed our Fe/GaAs microstructures in a way that allows us to reproduce these previous experiments and to simultaneously detect iSHE. Our work is related to experiments in Ref. [11] in which the SHE was electrically detected in Fe/$In_xGa_{1-x}As$ heterostructures.

Our Fe/n-GaAs heterostructure was grown epitaxially in a single molecular-beam-epitaxy chamber without breaking ultra high vacuum. The heterostructure comprises 250 nm of low Si-doped GaAs (5×10^{16} cm^{-3}), 15 nm of GaAs with graded doping, and 15 nm of highly Si-doped GaAs (5×10^{18} cm^{-3}). The doping profile yields a narrow tunnel Schottky barrier between GaAs and Fe favourable for spin injection/detection [16, 18–20]. The growth temcfperature of GaAs was 580°C. The sample was then cooled to 0°C for the growth of the 2 nm Fe layer. In the microdevice, the distance between Fe electrodes is 4 μm and between the Fe electrode and the Hall cross 2 μm (see Supplementary information). All measurements shown in this paper were performed at 4.2 K. Reproducibility was confirmed by performing measurements in three different samples with the same nominal heterostructure parameters and microdevice geometry and in each sample by contacting different combinations of available electrodes. To modulate the spin dependent signals at a constant spin injection current we apply an additional drift current along the channel.

The magnetic anisotropy of our Fe electrodes has a strong out-of-plane component (2 T) due to the thin-film shape anisotropy, the cubic magnetocrystalline component, and an additional uniaxial magnetocrystalline anisotropy originating from the broken [1$\bar{1}$0]/[110] symmetry of our ultrathin epitaxial Fe on GaAs. The anisotropies make the [110] crystal direction (y-axis in Fig. 1a) the easy magnetic axis with an anisotropy field of 0.2 T required to align the magnetization with the [1$\bar{1}$0] in-plane hard-axis. This anisotropy field is significantly larger than external magnetic fields applied in the Hanle precession experiments with typical amplitudes up to 50 mT. When these fields are applied along the in-plane hard-axis, the component of the magnetization along the easy-axis is reduced by less than 10%. The in-plane hard-axis Hanle geometry is suitable for the iSHE measurement because spins injected from the in-plane magnetized Fe electrode precess in GaAs out of the plane of the transport channel and because the ordinary (Lorentz force) Hall effect contributions can be experimentally separated in this set up [11]. This is essential for detecting iSHE in semiconductors. Only in the high carrier density metals, the ordinary Hall effect is relatively weak which allows to perform the iSHE experiments with out-of-plane oriented moments in the fer-

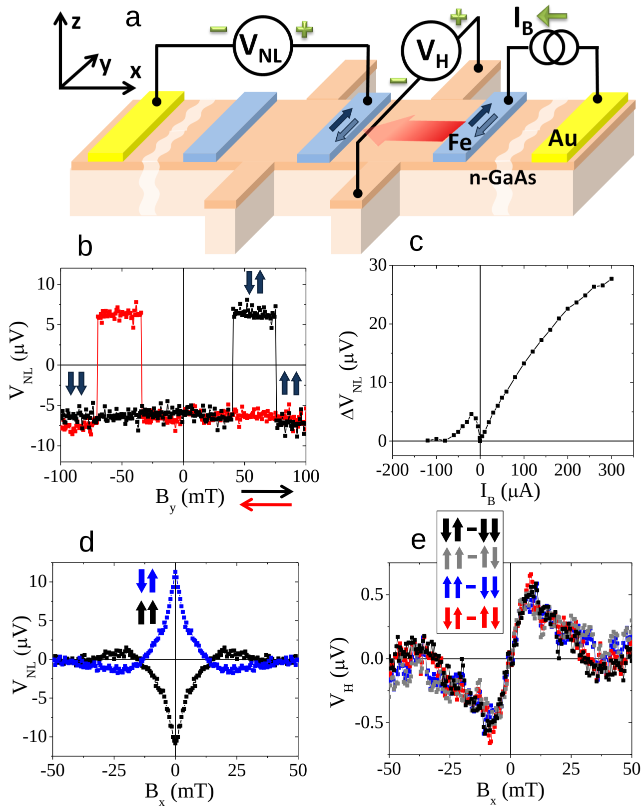

Figure 1: (a) Schematics of the device. (b)Non-local signal V_{NL} measured at bias-current $I_B = 100\ \mu$A in field B_y applied along the Fe easy-axis. The left (right) black arrow in each pair of arrows indicates the magnetization state of the detection (injection) Fe electrode. (c) The difference between V_{NL} at antiparallel and parallel configurations of magnetization in the injection and detection Fe electrode as a function of I_B. (d) Symmetrized Hanle measurement of V_{NL} at $I_B = 300\ \mu$A in hard-axis field B_x. (e) Antisymmetrized iSHE signal, V_H, under same experimental conditions as in (d).

romagnetic injection contact [13]. For characterizing individual Fe/GaAs Schottky contacts we performed three-point measurements between an individual Fe electrode and the two Au electrodes. By measuring the corresponding tunneling anisotropic magnetoresistance [22], we inferred the strength of the above anisotropy fields and the order in which the Fe electrodes switch their magnetization (see Supplementary information).

In Fig. 1b we plot the non-local spin-valve signal, V_{NL}, measured while sweeping the magnetic field B_y along the easy axis of the Fe electrodes. The field triggers magnetization reversal via domain nucleation and propagation process. The reversal fields are different in different Fe electrodes which allows us to control independently the magnetization orientations in the injection and detection electrodes. In the experiment, a bias current I_B driven between the injection (right) Fe/GaAs Schottky contact and the right Au electrode generates spin-accumulation underneath the spin-injection contact. A resulting diffusive spin-current propagates into the unbiased part of the semiconductor channel with the Hall cross and the detection (central) Fe electrode. The lower value of the non-local voltage, measured between the detection Fe electrode and the left Au electrode, corresponds to parallel orientations of magnetization of the injection and detection Fe electrodes; the higher value corresponds to antiparallel magnetizations. These data together with the dependence of the amplitude of the non-local voltage on the bias current I_B, plotted in Fig. 1c, reproduce previous results of spin injection experiments in GaAs channels with Fe Schottky contacts [11, 16, 18, 20, 21].

Non-local measurements on the Fe detection electrode in magnetic fields B_x applied along the Fe in-plane hard axis are shown in Fig. 1d. The black curve was obtained by setting the magnetizations in the Fe injection and detection electrodes in the parallel configuration before sweeping B_x; the blue curve was measured in the antiparallel magnetization configuration. At zero field we obtain the higher value of the non-local voltage for antiparallel magnetizations, consistent with Fig. 1b. The Hanle dependence of the non-local signal on B_x reflects the precession and dephasing of spins in the GaAs channel, as quantified in detail in the theory section. The injected spins precess in the plane perpendicular to B_x, i.e., acquire an out-of-plane component. Our observation of the iSHE signal in the GaAs is demonstrated in Fig. 1e. Consistent with the iSHE interpretation, the signal is zero at zero applied field since in this case the in-plane polarized injected spins do not precess in the GaAs channel. The variations of the iSHE signal in Fig. 1e and of the Hanle non-local signal in Fig. 1d occur at a comparable magnetic field scale. This confirms the precession origin of the out-of-plane spin component detected by iSHE.

The iSHE curves shown in Fig. 1e were obtained by subtracting the measured signals for oppositely preset polarizations of the Fe injection electrode before performing the Hanle measurement. The individual data measured for a given orientation of the injector polarization have a linear contribution from the ordinary Hall effect. The ordinary Hall contribution is independent of the orientation of the magnetization of the injection electrode and is experimentally removed by subtracting the data for opposite injector polarizations, as seen in Fig. 2a [11] (see Supplementary information). The signals shown in Fig. 1e and 2a are, therefore, of pure spin origin and are due to iSHE which is an odd function of the polarization of injected electrons. Since spin detection by iSHE is performed directly in the GaAs channel, the corresponding signal depends on the magnetization state of the Fe injection electrode and is independent of the other Fe electrodes. This behavior is confirmed in Fig. 1e which shows measurements for different magnetization configurations of the injection and detection electrodes.

For clarity, the Hanle non-local data shown in Fig. 1d

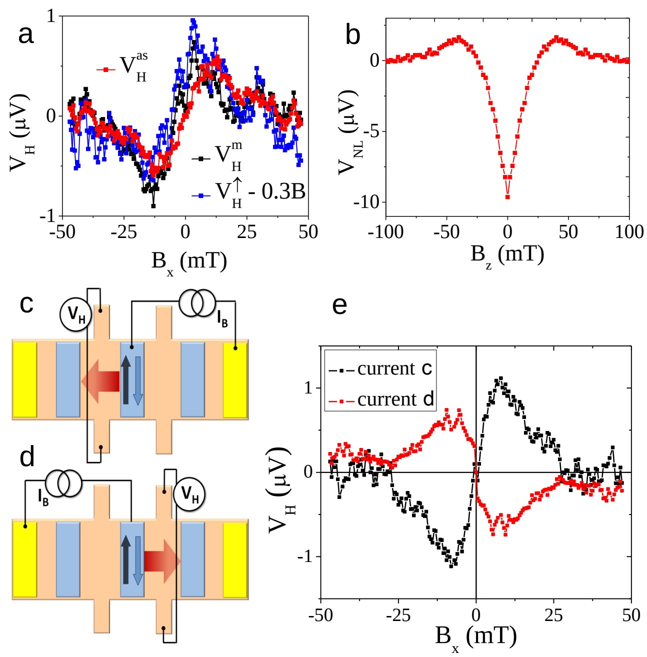

Figure 2: (a) The blue curve shows the measured raw data $V_H^{\uparrow}$, obtained by setting the magnetization in the Fe injection electrode in the positive easy-axis orientation, with a subtracted linear background of $0.3\mu V/\mathrm{mT}$. The black curve shows the pure spin signal V_H^m obtained by, $V_H^m = (V_H^{\uparrow} - V_H^{\downarrow})/2$. The red curve shows the antisymmetrized signal $V_H^{as}(B) = [V_H^m(B) - V_H^m(-B)]/2$. (b) Symmetrized V_{NL} measured in the out-of-plane hard-axis field B_z. (c),(d) Schematics of the experimental setups. (e) Antisymmetrized iSHE data for the in-plane hard-axis field measurements.

are symmetrized and, similarly, the iSHE data in Fig. 1e are antisymmetrized with respected to $B_x = 0$. In Fig. 2a we show that the antisymmetrization does not affect the key features of the iSHE measurements. Nevertheless, the absolute value of the raw data have a noticable asymmetry which we attribute to the presence of dynamic nuclear spin polarization effects [18–20]. Detailed measurements and discussion of the effects of the nuclear spins are presented in the Supplementary information. From the analysis we conclude that at slow enough sweep rates the Overhauser field produced by the nuclear spins [20] renormalizes the total effective field acting on electron spins as, $B_x^{eff} \approx 2B_x$ in case of the in-plane Hanle measurements. For the out-of-plane Hanle measurements, shown in Fig. 2b, the projection of the injected electron spins to the applied field B_z remains small. It yields negligible nuclear spin effects in this experimental geometry since the Overhauser field $\mathbf{B}_n \propto \left(\hat{\mathbf{B}} \cdot \langle \mathbf{P} \rangle\right) \hat{\mathbf{B}}$, where $\hat{\mathbf{B}}$ is the unit vector of the external magnetic field, $\langle \mathbf{P} \rangle = 2\langle \mathbf{s} \rangle / n$ is the mean electron spin polarization, $\mathbf{s}$ is the spin density, and n is the electron density in the channel.

In Fig. 2e we provide the consistency check of the sign of iSHE. We show measurements in which the sign of the spin-current is reversed by using the same Fe injection electrode but biasing it with the left or right Au contact. Corresponding experiments are sketched in Figs. 2c,d and the data plotted in Fig. 2e confirm that the sign of the measured Hall voltages is opposite for opposite orientations of the spin-current in the GaAs channel.

In experiments shown in Figs. 1 and 2, the spins in the GaAs are manipulated by the external magnetic field. The spin-current in these measurements is purely diffusive in the part of the GaAs channel between the injection and detection Fe electrodes. On the other side of the channel with the bias current I_B, both the diffusion and drift are present. In Fig. 3 we show measurements in which we apply a bias between the two Au electrodes causing an additional drift current component I_D on both sides of the injection electrode. I_B driven through the injection Fe electrode is kept constant (300 μA) while the additional current I_D is set to 0 and ± 100 μA. As seen in Figs. 3b,c, both the spin polarization measured underneath the Fe detection electrode and the spin-current measured by iSHE depend on I_D.

The data can be explained by a shift of the injected spin polarization profile from the injection electrode in the direction towards the Fe detection electrode in the case of $I_D = +100$ μA. In the experiment with $I_D = -100$ μA, the drift acts against diffusion on both sides of the injection electrode which makes the spin polarization profile decay more rapidly as we move away from the injection point. Our experiments use a method for modulating the output spin signal by electrical means which is distinct from the previous iSHE device with optical injection into a 2D GaAs channel [2]. The field applied across the dielectric, separating the 2D channel from a gate, controlled the spin precession via field dependent spin-orbit coupling [2]. In the present device, by applying the drift current, the non-uniform spin-polarization profile along the channel can be shifted and the corresponding spin-current increased or decreased which causes the electrically controlled modulation of the output signal. Note that the modulation by applied current was also used, e.g., in a Si spin channel in which case the electron transit time through the channel relative to the Hanle precession time in an external magnetic field was controlled by the current [23].

The spin dynamics in the GaAs channel can be modeled by the spin drift-diffusion equations. For the applied in-plane hard-axis field B_x, the spins precess in the $y-z$ plane and the corresponding Hanle curves are obtained by solving,

$$\frac{ds_{y/z}(x)}{dt} + \frac{d}{dx}\left(-D\frac{ds_{y/z}(x)}{dx} + v_d(x)s_{y/z}(x)\right) + \frac{s_{y/z}(x)}{\tau_s} + g\mu_B B_x^{eff} s_{z/y}(x) = \dot{S}_{y/z}\delta(x) \quad (1)$$

where $\dot{S}_y = \dot{S}_0$, $\dot{S}_z = 0$, and the nuclear Overhauser field is included in B_x^{eff}. Analogous equations apply for out-

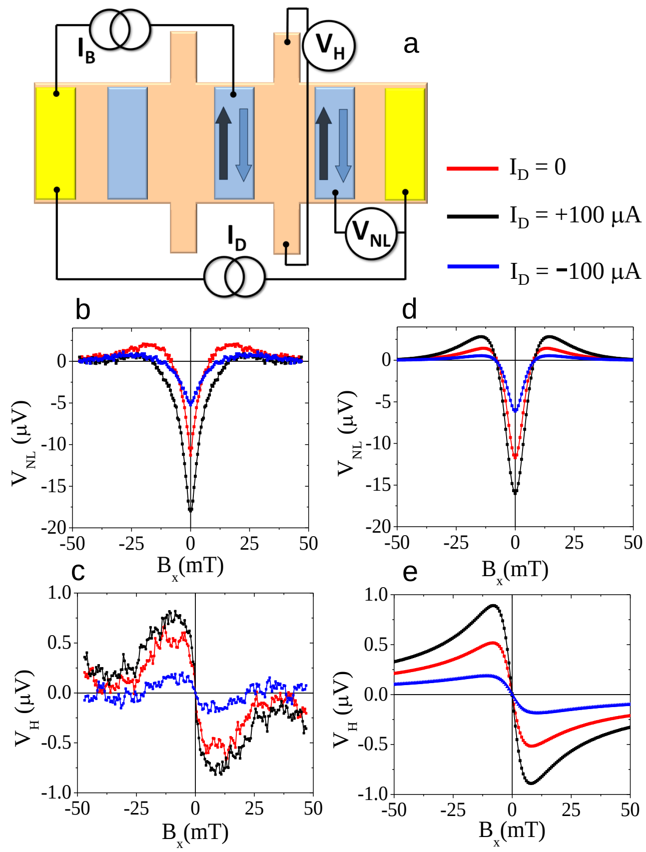

Figure 3: (a) Schematics of the experimental setup. (b),(c) Experimental symmetrized non-local spin valve and antisymmetrized iSHE signals in the in-plane hard-axis field measured at constant spin-injection bias current $I_B = 300\ \mu$A and at three different drift currents I_D depicted in (a). (d),(e) Calculations of the non-local spin valve and iSHE signals.

of-plane field B_z. In Eqs. (1), D is the diffusion constant, v_d is the drift velocity, τ_s is the spin-dephasing time, g is the Landé-factor of electrons in GaAs, and μ_B is the Bohr magneton. The right-hand side of Eq. (1) for the s_y component describes the rate of spins parallel to the Fe magnetic easy-axis ($\hat{y}$-axis) injected from the Fe contact to the GaAs channel at $x = 0$.

In our experiments, the drift velocity can be different on the right and left side of the injection electrode, $v_d(x) = \theta(x)v_d^R - \theta(x)v_d^L$, and is determined by the corresponding currents driven on either side of the injector. For a special case of $v_d^R = v_d^L$, the steady state spin density solving Eq. (1) is given by the commonly used expression [16],

$$s_y(x) = \int_0^\infty \frac{\dot{S}_0 dt}{\sqrt{4\pi Dt}} e^{-(x-v_d t)^2/4Dt - t/\tau_s} \cos(\omega_B t), \quad (2)$$

where $\omega_B = g\mu_B B_x/\hbar$. $s_z(x)$ is obtained by replacing cosine by sine.Assuming the step-like discontinuity in the drift velocity at the injection point, which corresponds to our experimental geometry, the solution of Eq. (1) outside the injection point must have the same functional form as the expression (2), up to a normalizing factor. The origin of the renormalization due to $v_d(x)$ with a sharp step at the injection point is that this form of $v_d(x)$ is equivalent to an additional source/sink term in the drift-diffusion equation at the injection point $(d\theta(x)/dx = \delta(x))$. As confirmed numerically , the two normalization factors for the right and left spin densities are obtained by matching the spin densities at the injection point and by requiring the same total integrated spin density as in the case of the constant drift velocity, i.e., $\int_{-\infty}^{\infty} dx s_y(x) = \tau_s \dot{S}_0/[1 + (\omega_B\tau_s)^2]$ and $\int_{-\infty}^{\infty} dx s_z(x) = \tau_s \dot{S}_0(\omega_B\tau_s)/[1+(\omega_B\tau_s)^2]$. This procedure is valid for spatially independent spin-dephasing time and magnetic field in Eq. (1).

The drift velocities corresponding to our experiments in Figs. 3b,c are given by, $v_d^R = I_D/enA$ and $v_d^L = (I_D + I_B)/enA$ (see Fig. 3a). Here e is the electron charge, n is the electron density in the GaAs channel, and A is the cross-sectional area of the channel. The diffusion constant is given by the expression for a degenerate semiconductor, $D = \mu_e n/eg(E_F)$, where μ_e is the electron mobility and $g(E_F)$ is the density of states at the Fermi level in GaAs conduction band with effective mass $m^* = 0.067$. The mobility $\mu_e = 3.5\times10^3$ cm^{2}V^{-1}s^{-1} and density $n = 1.1 \times 10^{17}$ cm^{-3}, and the corresponding diffusion constant $D = 2.9\times10^{-3}$ m^{2}s^{-1} and drift velocities were determined using the ordinary Hall measurements in the GaAs channel.

The spin-dephasing time $\tau_s = 1.65$ ns is obtained by matching the width of the theoretical and experimental Hanle curves. We determined τ_s from measurements in the applied out-of-plane hard-axis field B_z, i.e., in the geometry where the Overhauser field is negligible. The remaining input parameter needed for obtaining the quantitative values of the theoretical non-local Hanle curves, shown in Fig. 3d, is the overall normalization factor of the continuous solution of Eq. (1) (or equivalently the value of $\dot{S}_0$). This is obtained by matching the theoretical and experimental spin densities in GaAs underneath the detection electrode. The experimental value is inferred from the difference between the zero field non-local spin valve voltages at parallel and antiparallel magnetization configurations of the injection and detection Fe electrodes considering [16], $\Delta V_{NL} = 2\eta P_{\rm Fe} P_{\rm GaAs} E_F/3e$. Here $\eta = 0.5$ is the spin transmission efficiency of the interface, $P_{\rm Fe} = 0.42$ is the polarization of the Fe electrode, and $P_{\rm GaAs} = 2s_y(x_d)/n$ is the polarization in GaAs underneath the Fe detection electrode ($x = x_d$).

The iSHE is proportional to the $\hat{z}$-component of the spin-current given by $j_z^s(x) = -D\vec{\nabla}s_z(x) + v_d(x)s_z(x)$. Since $j_z^s(x)$ depends on the spatial coordinate we have to consider also the response function $F_{cross}(x)$ of the finite-size Hall cross when interpreting the experiments. We performed the numerical evaluation of $F_{cross}(x)$ for our sample geometry using the conformal mapping theory (see Supplementary information). The measured iSHE signal is then proportional to $J_z^s = \int_{-\infty}^{\infty} dx j_z^s(x) F_{cross}(x) / \int_{-\infty}^{\infty} dx F_{cross}(x)$. The spin-current and the iSHE voltage are related as, $V_H = ew\alpha J_z^s/\sigma$, where α is the spin Hall angle and $\sigma = ne\mu_e$ is the electrical conductivity of the GaAs channel. The theoretical V_H plotted in Fig. 3e is obtained by taking $\alpha = 1.5 \times 10^{-3}$ which is a value consistent with the estimates of the skew-scattering Hall angle for the disordered weakly spin-orbit coupled GaAs channel (see Supplementary information). The value is also consistent with spin Hall angles in diffusive GaAs channels reported in optical and electrical spin Hall measurements [8, 11, 24]. Figs. 3b,d and 4c,e demonstrate the agreement we obtain between the measured and calculated non-local spin valve and iSHE voltages. The theory successfully describes the dependence of the measured spin signals on both the applied magnetic field and on the applied electrical drift current.

We acknowledge EU grants ERC 268066-0MSPIN, FP7-215368 SemiSpinNet, from Czech Republic grants AV0Z10100521, and Preamium Academiae, and from U.S. grants ONR-N000141110780, NSF-MRSEC DMR-0820414, NSF-DMR-1105512, and NHARP.

[1] J. Wunderlich *et al.*, Nature Phys. **5**, 675 (2009).
[2] J. Wunderlich *et al.*, Science **330**, 1801 (2010).
[3] M. I. Dyakonov and V. I. Perel, JETP Lett. p. 467 (1971).
[4] J. E. Hirsch, Phys. Rev. Lett. **83**, 1834 (1999).
[5] S. Zhang, Phys. Rev. Lett. **85**, 393 (2000).
[6] S. Murakami, N. Nagaosa, and S.-C. Zhang, Science **301**, 1348 (2003),
[7] J. Sinova *et al.*, Phys. Rev. Lett. **92**, 126603 (2004).
[8] Y. K. Kato, R. C. Myers, A. C. Gossard, and D. D. Awschalom, Science **306**, 1910 (2004).
[9] J. Wunderlich, B. Kaestner, J. Sinova, and T. Jungwirth, Phys. Rev. Lett. **94**, 047204 (2005).
[10] T. Kimura *et al.*, Phys. Rev. Lett. **98**, 156601 (2007).
[11] E. S. Garlid *et al.*, Phys. Rev. Lett. **105**, 156602 (2010).
[12] E. Saitoh, M. Ueda, H. Miyajima, and G. Tatara, Appl. Phys. Lett. **88**, 182509 (2006).
[13] S. O. Valenzuela and M. Tinkham, Nature **442**, 176 (2006).
[14] H. Zhao, E. J. Loren, H. M. van Driel, and A. L. Smirl, Phys. Rev. Lett. **96**, 246601 (2006).
[15] C. Brüne *et al.*, Nature Phys. **6**, 448 (2010).
[16] X. Lou *et al.*, Nature Phys. **3**, 197 (2007).
[17] M. Ciorga *et al.*, Phys. Rev. **B 79**, 165321 (2009).
[18] C. Awo-Affouda *et al.*, Appl. Phys. Lett. **94**, 102511 (2009).
[19] M. K. Chan *et al.*, Phys. Rev. **B 80**, 161206 (2009).
[20] G. Salis, A. Fuhrer, and S. F. Alvarado, Phys. Rev. **B 80**, 115332 (2009).
[21] G. Salis *et al.*, Phys. Rev. **B 81**, 205323 (2010).
[22] J. Moser *et al.*, Phys. Rev. Lett. **99**, 056601 (2007).
[23] B. Huang, D. J. Monsma, and I. Appelbaum, Appl. Phys. Lett. **91**, 072501 (2007).
[24] S. Matsuzaka, Y. Ohno, and H. Ohno, Phys. Rev. **B 80**, 241305(R) (2009).